Homoclinic bifurcation in Chua's circuit

S K DANA[1], S CHAKRABORTY[2] and G ANANTHAKRISHNA[3]

[1,2]Instrument Division, Indian Institute of Chemical Biology, Kolkata 700 032, India
[3]Material Research Centre and Centre for Condensed Matter Physics, Indian Institute of Science, Bangalore 560 016, India
E-mail: skdana@iicb.res.in; satya_iicb@yahoo.com; garani@mrc.iisc.ernet.in

Abstract. We report our experimental observations of the Shil'nikov-type homoclinic chaos in asymmetry-induced Chua's oscillator. The asymmetry plays a crucial role in the related homoclinic bifurcations. The asymmetry is introduced in the circuit by forcing a DC voltage. For a selected asymmetry, when a system parameter is controlled, we observed transition from large amplitude limit cycle to homoclinic chaos via a sequence of periodic mixed-mode oscillations interspersed by chaotic states. Moreover, we observed two intermediate bursting regimes. Experimental evidences of homoclinic chaos are verified with PSPICE simulations.

Keywords. Chua's circuit; asymmetry; mixed mode oscillations; homoclinic chaos; bursting.

PACS No. 05.45

1. Introduction

Homoclinic orbit is asymptotic to a saddle limit set both forward and backward in time [1,2]. In the vicinity of the homoclinic orbit, if a control parameter is tuned to the bifurcation point, there exists a countable infinity of periodic orbits, which are at the origin of chaos in nonlinear dynamical system. The homoclinic orbit is structurally unstable and difficult to observe in experiments. However, homoclinic chaos of the Shil'nikov-type has been observed in BZ reaction [3], liquid crystal flow [4], CO_2 laser [5,6], optothermal bistable device [7] and electronics [8]. The trajectory of homoclinic chaos switches irregularly between firing state and quiescent state. The geometry of homoclinic chaos appears regular globally yet instabilities are bounded to a local domain close to the saddle, which may be a saddle focus or a saddle cycle in 3D system. The local instability has its manifestation in large fluctuations in the return time of the spiking oscillation. It has striking similarities with spiking of neurons [9,10]. In fact, homoclinic bifurcation is considered, in recent times [11–13], as one of the important mechanism of the emergence of spiking and bursting behaviors of neurons. Recent experiments [14] on message encoding using phase synchronization of external signal in the interspike intervals

of homoclinic chaos in CO_2 laser have explored the potential of homoclinic chaos as a suitable candidate of message encoding for secure communication.

The Shil'nikov scenario [1,2] deals with a saddle focus with real and complex conjugate eigenvalues, $(\sigma \pm j\omega, \gamma)$ in 3D systems. The homoclinic orbit escapes spirally from the saddle in 2D eigensapce and re-injects into it along the stable eigendirection for $\gamma < 0$ and $\sigma > 0$ and if it satisfies the condition $|\gamma/\sigma| > 1$. In period-parameter space, the period of a limit cycle (period-n: $n^0, n = 1, 2, 3...$) increases asymptotically with a control parameter as it approaches the homoclinic orbit. Further studies [15] on Shil'nikov chaos show later that a Shil'nikov wiggle appears in period-parameter space if $1/2 < |\gamma/\sigma| < 1$ for $\gamma < 0$ and $\sigma > 0$. When a control parameter is tuned from both sides of the homoclinic point, the period of a limit cycle increases in a wiggle with alternate sequences of stable and unstable orbits via saddle-node (SN) and period-doubling (PD) bifurcation respectively.

In nonlinear systems, the dynamics usually changes with a parameter from stable equilibrium to limit cycle by super-Hopf bifurcation and to chaos via PD. With further changes in parameter, the system shows period-adding bifurcation when a sequence of periodic windows appears intermediate to chaotic windows. The periodic windows are created via SN bifurcation while the chaotic states appear via PD. Subsequently, the dynamics follows a reverse PD before moving to unstable limit cycle via sub-Hopf bifurcation.

Several numerical studies [16–19] showed evidences of mixed mode oscillations (MMOs) as a transition route to the Shil'nikov-type homoclinic chaos with control parameter in slow–fast systems. A sequence of MMOs is observed in the intermediate periodic regimes of the bifurcation diagram of the system, which again exist in isolated bifurcation curves (isolas) as elaborated in [3,17] and most recently in a jerky flow model [19]. The MMO as illustrated in Boissonade–De Kepper model [17,18] arises at a point when a large amplitude limit cycle loses stability via SN bifurcation. It is seen as transition from large-amplitude limit cycle to Farey sequences of periodic MMO, $1^0 \rightarrow \infty^1 \rightarrow n^1 \rightarrow 1^n \rightarrow 1^\infty$ (n is an integer), interspersed by narrow chaotic states when a control parameter is tuned to homoclinicity. 1^0 denotes the large-amplitude limit cycle (period-1) while α^1 denotes a periodic orbit with transition to small oscillation for once in a long run. The alternate sequences of periodic and chaotic MMOs appear via SN and PD bifurcations respectively. The MMOs are usually denoted by L^s, where L and s are the number of large- and small-amplitude oscillations respectively. L remains fixed for a set of selected system. The number of small oscillations (s) is stable in a periodic window but it is highly irregular in chaotic windows. For different sets of selected parameters, MMO of higher L $(= 2, 3, ...)$ may also be observed. It is noteworthy that the width of both the periodic and chaotic windows become narrower when the control parameter is tuned to the homoclinic point. As the control parameter approaches the homoclinic point, the number of small oscillations increases while the trajectory moves closer and closer to the saddle. The state of homoclinic chaos denoted by 1^∞ $(L = 1)$ is reached when the small oscillations s become finitely very large but highly irregular. The number of small oscillations (s) is highly irregular in the chaotic windows, which is reflected as large fluctuations in return time of homoclinic spiking. The homoclinic chaos thus may be seen as infinite number of unstable MMOs embedded into it.

In this paper, we report our experimental observations of the Shil'nikov-type homoclinic chaos in Chua's circuit from the viewpoint of induced asymmetry. The original Chua's circuit model has reflection symmetry. Experiments are described here to show that the asymmetry deliberately induced in a Chua's circuit, can be controlled to find many complex features, such as mixed mode oscillation and bursting. In real systems, several sources of imperfection always exist, which break the reflection symmetry of a model system. These imperfections are usually modeled [20] by an additional constant term to the normal form of a model flow. Using this concept, we induced asymmetry in a single Chua's circuit by forcing a DC voltage to investigate the role of asymmetry in the origin of homoclinic chaos. We observed sequences of MMOs interspersed by chaotic windows during the intermediate stages of transitions from one large-amplitude limit cycle to another large-amplitude limit cycle with a control parameter. The dynamics follows the sequence of transitions $n^0 \to \infty^1 \to n^1 \to n^m \to L^s \to n^p \to n^1 \to \infty^1 \to n^0$ (n, m and p are integers) when a system parameter is controlled keeping the asymmetry parameter at suitably selected value. We are able to observe at least two different scenarios of MMO (L^s: $L = 1, 2$) in the process of transition to homoclinic chaos for two different sets of selected parameters. Evidences of two intermediate bursting regimes ($n^1 \to n^m$ and $n^p \to n^1$) are observed for each scenario at the edges of transition from one large-amplitude limit cycle to MMO and from MMO to the other large-amplitude limit cycle. Many more scenarios with larger L may be observed by appropriate choice of system parameters and asymmetry parameter.

The text of this paper is organized as follows: In the next section, we described the experimental set-up. Evidences of homoclinic chaos and bursting are elaborated in §3. Details of observed MMO are presented in §4. The results are summarized with a conclusion in §5.

2. Experimental set-up: Asymmetric Chua's circuit

We forced a DC voltage to C_1 capacitor node in a Chua's circuit shown in figure 1 to induce asymmetry in the attractor. The model of the asymmetry-induced Chua's circuit is given by

$$\frac{dV_{C_1}}{dt} = \frac{G}{C_1}(V_{C_2} - V_{C_1}) - \frac{1}{C_1}f(V_{C_1}) + \frac{1}{R_C C_1}(V_0 - V_{C_1})$$

$$\frac{dV_{C_2}}{dt} = \frac{1}{C_2}[I_L - G(V_{C_2} - V_{C_1})]$$

$$\frac{dI_L}{dt} = -\frac{1}{L}(V_{C_2} + r_0 I_3) \tag{1}$$

and

$$f(V_{C_1}) = \begin{vmatrix} G_b V_{C_1} + (G_b - G_a)E & \text{if } V_{C_1} < -E \\ G_a V_{C_1} & \text{if } E \le V_{C_1} \le E, \\ G_b V_{C_1} + (G_a - G_b)E & \text{if } V_{C_1} > E \end{vmatrix} \tag{2}$$

where $G = 1/R_1$ and G_a, G_b are the slopes in the inner and outer regions [21–23] respectively of the piece-wise linear characteristic $f(V_{C_1})$. The slopes G_a and G_b
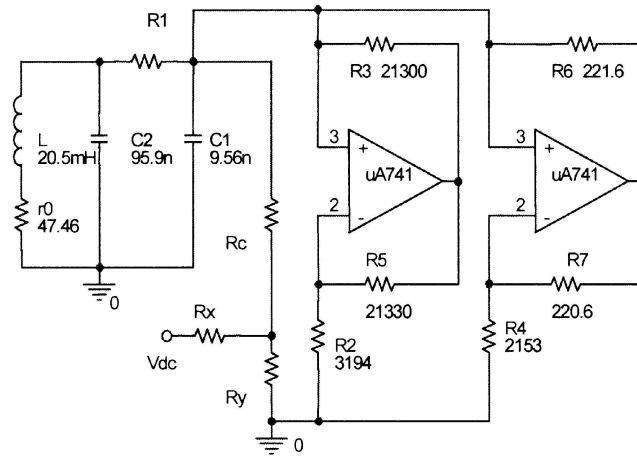
Figure 1. Asymmetric Chua's oscillator: ±9 V supply.

are determined by

$$G_a = \left(-\frac{1}{R_2} - \frac{1}{R_4}\right), \quad G_b = \left(\frac{1}{R_3} - \frac{1}{R_4}\right). \tag{3}$$

The state variables V_{C_1}, V_{C_2}, and I_L are the voltages measured at the nodes of capacitors C_1 and C_2, and the current through the inductance L respectively. The DC source V_{DC} is connected to the Chua's circuit using a voltage divider with resistances R_x and R_y, where $V_0 = V_{DC}(1 + \frac{R_x}{R_y})$. To facilitate fine control over the strength of asymmetry, a series resistance R_C is connected between the voltage divider and the Chua's circuit. The symmetric Chua's circuit (no DC forcing) shows [21–23] transition from limit cycle to single scroll chaos via PD and then to alternate period adding and chaotic states via saddle-node (SN) and PD bifurcation respectively, and finally to double scroll chaos. The original model has three saddle foci, one near the origin with eigenvalues $(\gamma, -\sigma \pm j\omega)$ and other two at reflection symmetric positions with eigenvalues $(-\gamma, \sigma \pm j\omega)$. The trajectory of double scroll in Chua's circuit revolves most of the time near either of the mirror symmetric equilibrium points and switches irregularly between the two. Thus the system shows two time-scales inherent in the dynamics of Chua's double scroll attractor, one due to the single scroll oscillation near either of the saddle foci and other due to a large cycle around both the equilibrium points. This is atypical of a dynamical system with piece-wise linear characteristics spreading over three regions. By inducing asymmetry in the double scroll Chua's oscillator one of the single scroll shrinks in size thereby two different time-scales are introduced, which characterize a large-amplitude oscillation and a small-amplitude oscillation. Effectively, the asymmetry in the double scroll attractor appears with a shift of the saddle focus near the origin closer to the saddle focus at one end than that at the other end. However, the basic nature of the eigenvalues of all saddle foci as noted above remain unchanged in our experimental parameter setting.
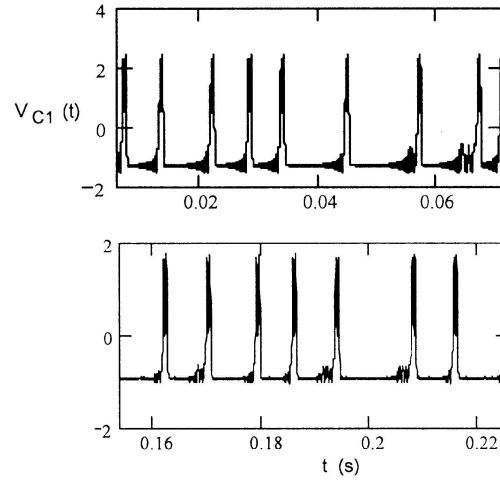
Figure 2. Homoclinic chaos in asymmetry-induced Chua's circuit. Time series of PSPICE simulation for $L = 2$ in the upper plot for $R_1 = 1429.9$ Ω, $R_C = 45$ kΩ, $R_x = 1580$ Ω, $R_y = 507$ Ω and of experiment for $R_1 = 1370.1$ Ω, $R_C = 47.25$ kΩ, $R_x = 9.33$ kΩ, $R_y = 1.73$ kΩ in the lower plot.

3. Homoclinic chaos and bursting

The asymmetry in the Chua's circuit is controlled by the combination of resistance R_x, R_y and R_C. The resistance R_C is used only to control the asymmetry in the attractor, once the resistance R_x and R_y are appropriately selected. For selected system parameter R_1 and asymmetry parameter R_C, the time series from both experiment and PSPICE simulation are shown in figure 2, which show clear evidences of homoclinic chaos for $L = 2$ as a train of high-amplitude spikes with irregular switching to quiescent state. The time series of homoclinic chaos may be seen here as MMO (2^s: $L = 2$) with highly fluctuating number of small-amplitude oscillations (s). The number of small-amplitude oscillations decides the time interval of the large-amplitude spiking, whose successive time intervals are highly uncorrelated. It may be mentioned here again that the homoclinic trajectory reaches as close to the saddle as the number of small oscillations increases. A fine tuning of the R_C value is necessary, at this point, to obtain a critical value in close proximity to homoclinicity so as to maximize the number of small oscillations with large fluctuations in the interspike intervals. The corresponding 3D trajectories are shown in figure 3 as obtained from PSPICE simulation and experiment. The trajectory moves towards the saddle focus at one end along its stable eigendirection as indicated by the arrows in figure 3. When the trajectory comes in close proximity to this saddle focus, it escapes from it in spirals. Next it spirals in towards the middle saddle focus before totally escaping from this unstable domain along the unstable eigendirection of this saddle. Finally the trajectory takes two global turns before reinjecting again into the first saddle focus. In reality, the trajectory of the 3D unstable orbit approaches homoclinicity in two different saddle foci, one in the middle and the other at one end of the attractor.
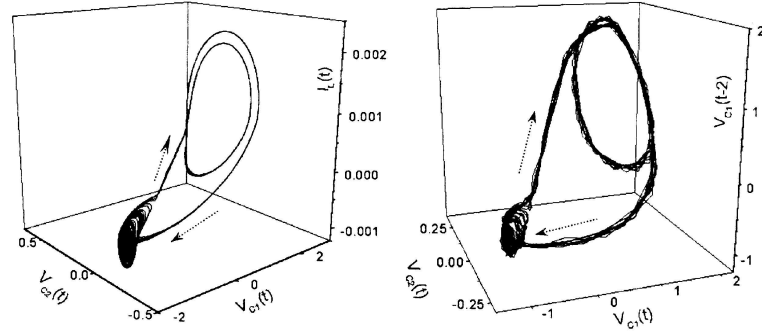
Figure 3. The 3D trajectory of homoclinic chaos. Left plot from PSPICE simulation using time series of $I_L(t)$, $V_{C_2}(t)$ and $V_{C_1}(t)$ for $L = 2 : R_1 = 1429.9$ Ω, $R_C = 45$ kΩ, $R_x = 1580$ Ω, $R_y = 507$ Ω. Right plot from experimental time series of $V_{C_1}(t)$, $V_{C_2}(t)$ and delayed $V_{C_1}(t-2)$ using embedding technique: $R_1 = 1370.1$ Ω, $R_C = 47.25$ kΩ, $R_x = 9.33$ kΩ, $R_y = 1.73$ kΩ.
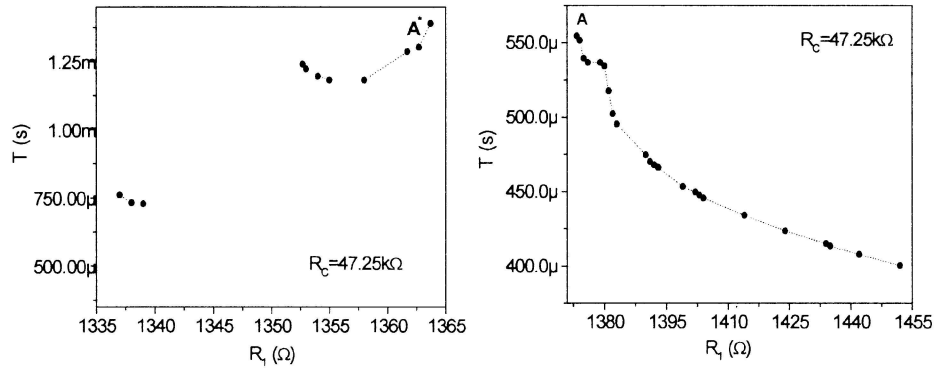

Figure 4. Period parameter bifurcation. $R_C = 47.25$ kΩ, $R_x = 9.33$ kΩ, $R_y = 1.73$ kΩ.

In our first experiment, we set the asymmetry by $R_x = 9.33$ kΩ, $R_y = 1.73$ kΩ and $R_C = 47.25$ kΩ, and then decrease R_1 from 1524 Ω. As R_1 is decreased, the circuit dynamics moves from stable focus to limit cycle via super-Hopf bifurcation at $R_1 = 1524$ Ω and a transition to 2-band chaos occurs via a sequence of PD. A large-amplitude limit cycle of period-2 (2^0) appears via reverse PD at $R_1 = 1373.3$ Ω as shown in figure 5 (plot in upper row left). The period–parameter bifurcation in figure 4 (right diagram) shows asymptotic increase in period with decrease in R_1 indicating an approach to homoclinicity. The large-amplitude limit cycle 2^0 for $R_1 = 1373.3$ Ω is seen at the highest point (A) of the bifurcation diagram. The dynamical behavior shown by the phase portrait in figure 5 (upper row left) first attains an imperfect homoclinicity to the middle saddle, in the sense of the discussion in previous section, before losing stability. The instability started just beyond this point with further decrease in R_1 until at $R_1 = 1363.7$ Ω when it stops with the re-appearance of the large-amplitude limit cycle (2^0) shown in figure 5 (plot
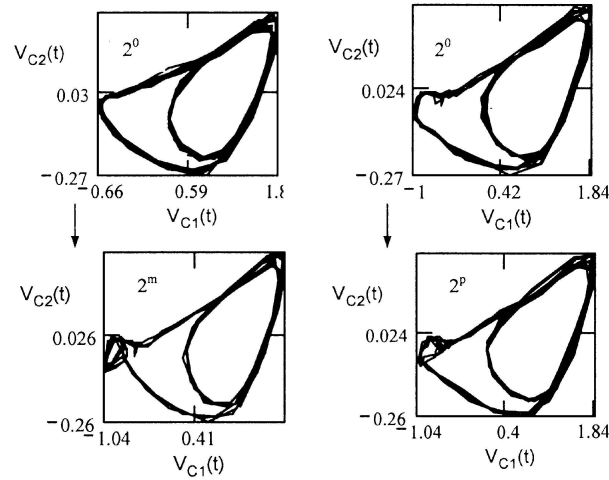
Figure 5. Phase portraits of $V_{C_1}(t)$ vs. $V_{C_2}(t)$. Upper row: Large-amplitude limit cycles for $R_1 = 1373.3\ \Omega$ (left) and for $R_1 = 1363.7\ \Omega$ (right). Lower row: Unstable small-amplitude limit cycle glued to the stable large-amplitude limit cycle via SN bifurcation for $R_1 = 1373.2\ \Omega$ (left) and for $R_1 = 1364\ \Omega$ (right).

in upper row right) corresponding to the top (A^+) of the left bifurcation diagram in figure 4. The second large amplitude also attains imperfect homoclinicity to middle saddle in a sense similar to the first large-amplitude limit cycle. The period in left plot (figure 4) then decreases with R_1. But the period increases again with an intermediate minimum until another instability region appears at $R_1 = 1352.3$ Ω. A stable limit cycle (period-2) appears again at $R_1 = 1339\ \Omega$, which moves to 1^0 (period-1) limit cycle at $R_1 = 1337\ \Omega$ via reverse PD and finally loses stability via sub-Hopf bifurcation for $R_1 < 1337\ \Omega$. Each of the local maximum in the period–parameter bifurcation indicates an approach to homoclinicity. However, it is difficult to identify them in a single experiment due to their extreme sensitivity to control parameter. We concentrated, in the first experiment on evidences of homoclinicity related to MMO (2^s) in the R_1 interval of (1363.7 Ω, 1373.3 Ω). In this parameter interval, $R_1 = (1363.7\ \Omega, 1373.3\ \Omega)$ several complex behaviors like bursting and MMO and homoclinic chaos are observed. The large-amplitude limit cycles (2^0) called as spiking at both the edges (A, A^+) of the R_1(1363.7 Ω, 1373.3 Ω) interval are shown in the upper row of figure 5. The time series of spiking large-amplitude limit cycles at the edges are shown in figure 6. For small changes in $R_1 = 1364\ \Omega$ (right : 2^p) and 1373.2 Ω (left : 2^m) near these edges, two bursting oscillations appear by the loss of stability in each of the large-amplitude limit cycle as shown in the lower phase portraits in figure 5. The corresponding time series of bursting oscillations are shown in figure 7. The bursting oscillations are seen here as a train of periodic spiking with intermittent transition to small oscillations. During bursting, the number of large spikes is also irregular between intermittent small-amplitude oscillations. The unstable small-amplitude limit cycle (2^m) appears in figure 5 as glued (lower row left) to the stable large-amplitude limit cycle via SN
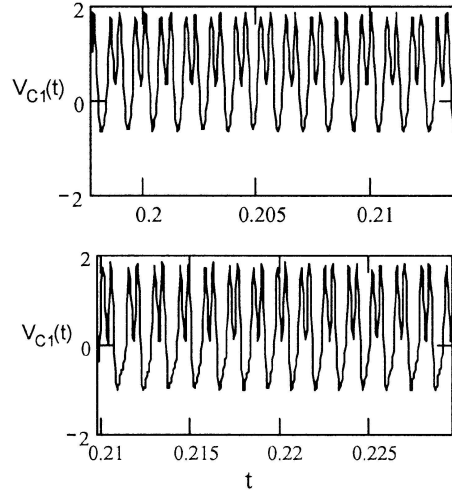
Figure 6. Time series of $V_{C_1}(t)$ for large amplitude limit cycles. For $R_1 = 1373.3\ \Omega$, $1363.7\ \Omega$ in the upper and lower plots respectively at the edges of the instability interval.
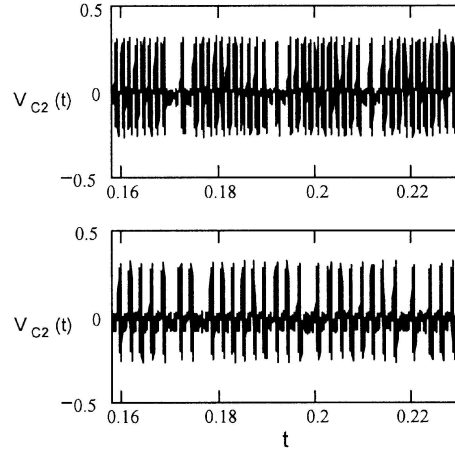
Figure 7. Time series of bursting oscillations for $R_1 = 1364\ \Omega$ (2^p) in the upper plot and for $R_1 = 1373.2\ \Omega$ (2^m) in the lower plot.

bifurcation while it is inside the large limit cycle for 2^p. We also observed a sequence of MMOs interspersed by chaotic states in the parameter interval of $R_1 = (1363.7\ \Omega, 1373.3\ \Omega)$ as a route to homoclinic chaos (2^s) for $R_1 = 1370.1\ \Omega$ already shown in figures 2 and 3. However, it becomes very difficult to identify the periodic MMOs, in this experiment, due to their extremely narrow interval in the selected parameter space.

In a second experiment, by appropriate choice of system parameters and control of the asymmetry parameter, we observed a sequence of transitions $1^0 \rightarrow \infty^1 \rightarrow 1^1 \rightarrow 1^m \rightarrow 1^s \rightarrow 1^p \rightarrow 1^1 \rightarrow \infty^1 \rightarrow 1^0$. The large-amplitude limit cycle is period-1 (1^0) here. We observed the sequence of transitions as large-amplitude limit cycle (1^0), bursting (1^m), homoclinic chaos (1^s), and then again bursting (1^p), large-amplitude limit cycle (1^0) with changes in R_1 as shown in figure 8. The phase portraits of the five different states are shown in figure 9.

4. Mixed mode oscillation

We chose a different set of parameters, $R_x = 1858\ \Omega$, $R_y = 333\ \Omega$, in a separate experiment and find similar sequence of events as described above but with clear evidences of periodic MMO. For selected $R_C = 47.14\ \text{k}\Omega$, the parameter $R_1 = 1357\ \Omega$ is critically tuned to observe homoclinic chaos as shown in figure 10. We observed the sequences of periodic MMOs with intermediate chaotic states when R_C is increased to $85\ \text{k}\Omega$ keeping other parameters unchanged. The period–parameter bifurcation in figure 11 shows devil's staircases with asymptotic increase in period
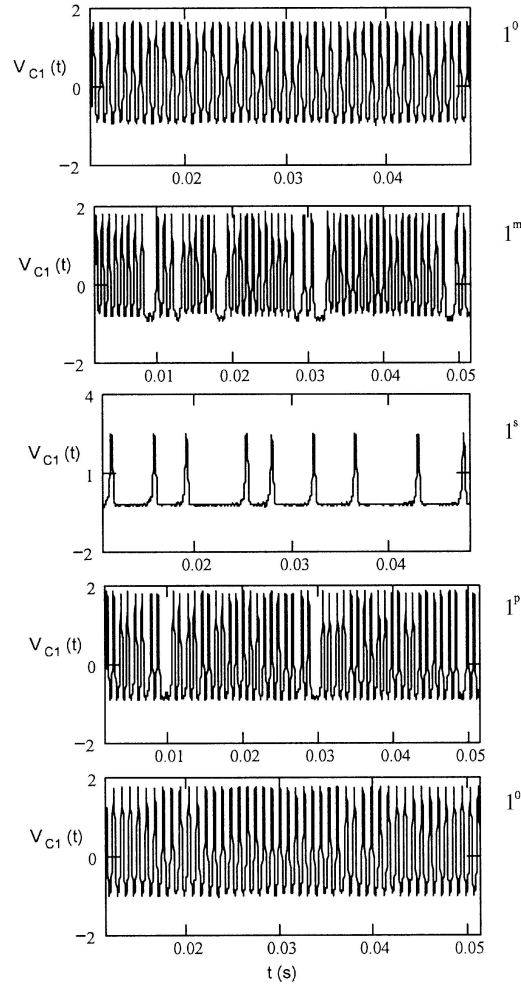
Figure 8. Time series of transitional phases to homoclinic chaos ($L = 1$). Top to bottom, $R_1 = 1334.1\ \Omega\ (1^0)$, $1334\ \Omega\ (1^m)$, $1333.3\ \Omega\ (1^s)$, $1332\ \Omega\ (1^p)$, $1331.5\ \Omega\ (1^0)$, for $R_x = 4.2$ kΩ, $R_y = 1.6$ kΩ and $R_C = 80.2$ kΩ.

while approaching homoclinicity with decease in R_C. We are able to observe a sequence of periodic MMOs (2^s) with a maximum number of small oscillations $s = 10$ for $R_C = 55$ kΩ. The interval in R_C parameter for the MMO becomes narrower with increasing small oscillations (s) as reported earlier for other systems [3,16–19]. The intervals between the line plots in figure 11 indicate the chaotic windows. It is important to note that the time period of the largest (2^{10}) MMO is nearly 5 ms for $R_C = 55$ kΩ while the time series of homoclinic chaos in figure 10 for $R_C = 47.14$ kΩ show fluctuations in the interspike intervals between 8 ms and 16 ms. It is clearly evident that as R_C is slowly tuned from 55 kΩ (corresponding to the largest MMO ($s = 10$)) to 47.14 kΩ, the interpsike intervals increase three-fold.
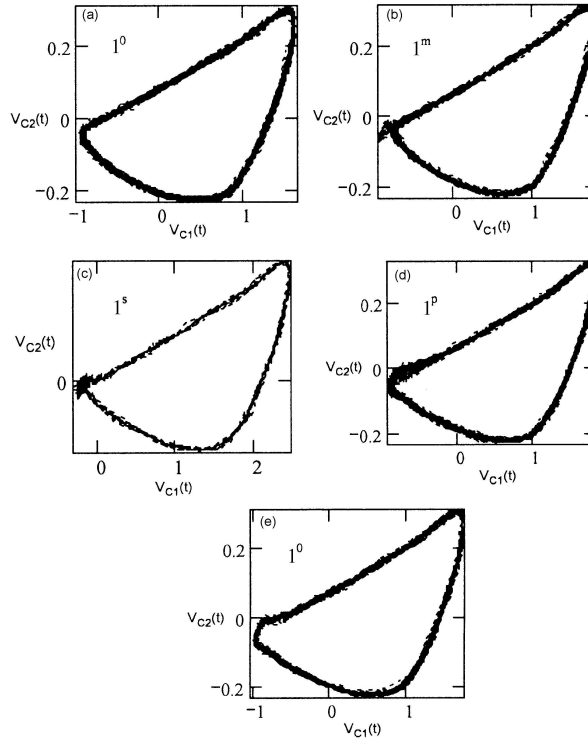
Figure 9. Phase portraits of transitional phases of 1^0 limit cycle: (**a**) $R_1 = 1334.1 \ \Omega \ (1^0)$, (**b**) 1334 Ω (1^m), (**c**) 1333.3 Ω (1^s), (**d**) 1332 Ω (1^p), (**e**) 1331.5 Ω (1^0) for $R_x = 4.2$ kΩ, $R_y = 1.6$ kΩ and $R_C = 80.2$ kΩ.

Thus, by fine tuning the asymmetry parameter, we are able to reach a close vicinity of the homoclinic orbit with much larger $(s \gg 10)$ number of small oscillations. The time series of periodic MMOs are shown in figure 12. The y-scale is arbitrarily chosen since different time series are either scaled up or down for visual clarity.

5. Conclusion

We find experimental evidences of homoclinic chaos in asymmetry-induced Chua's oscillator. The asymmetry plays a crucial role in homoclinic bifurcations in the process of transition to homoclinic chaos and away from it, when we observed spiking, bursting and MMO. When a system parameter is changed for selected asymmetry, the large-amplitude limit cycle (n^0: $n = 1, 2$) moves to MMO through a bursting region $(n^1 \rightarrow n^m)$ via SN bifurcation. The system then moves to periodic MMOs with increasing number of small oscillations interspersed by chaotic states. Homoclinic chaos is observed, in this MMO regime, when the asymmetry parameter is fine tuned. The system moves to another large-amplitude limit cycle with further change in system parameter. During this later transition, another bursting region
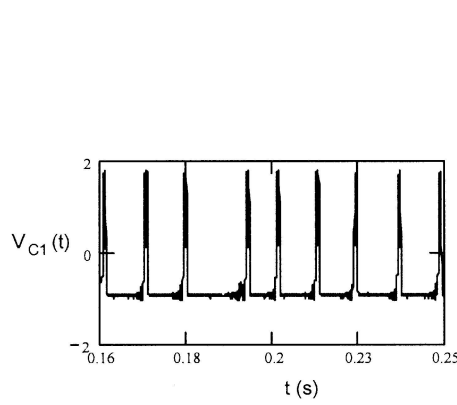
Figure 10. Homoclinic chaos. $R_1 = 1357$ Ω, $R_x = 1858$ Ω, $R_y = 333$ Ω and $R_C = 47.14$ kΩ.
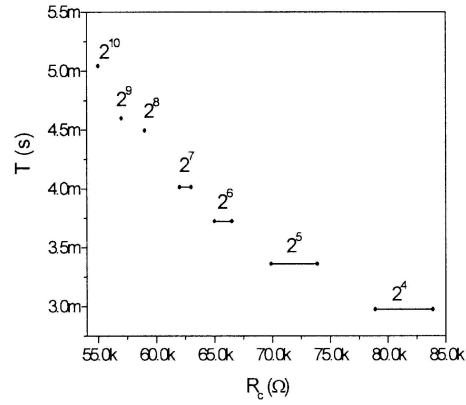
Figure 11. Period parameter bifurcation: $R_1 = 1357$ Ω and $R_x = 1858$ Ω, $R_y = 333$ Ω. Period of periodic mixed mode oscillations are plotted, intervals are noted as chaotic states.
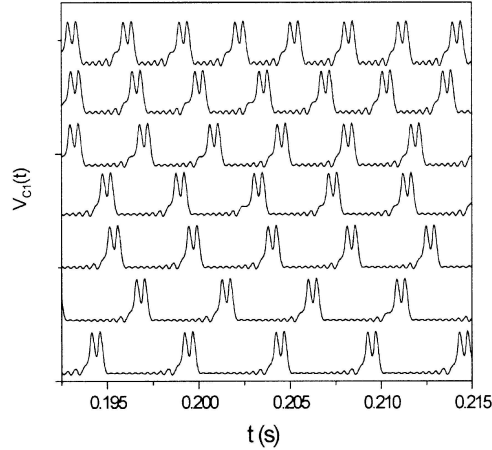
Figure 12. Mixed mode oscillations. $R_1 = 1357$ Ω and $R_x = 1858$ Ω, $R_y = 333$ Ω. Mixed mode oscillations from top to bottom for $L = 2$ and $s = 4, 5, 6, 7, 8, 9, 10$. R_C values are 78.9 kΩ, 69.9 kΩ, 65 kΩ, 62 kΩ, 59 kΩ, 57 kΩ and 55 kΩ respectively.

$(n^p \rightarrow n^1)$ is also observed. The existence of this second bursting regime on the way back to large limit cycle from homoclinic chaos is overlooked in earlier works. However, the emergence of MMO from large-amplitude limit cycle via a bursting regime followed by the transition to homoclinicity has been reported earlier in slow–fast system models.

To the best knowledge of the authors, homoclinic chaos is investigated, in this paper, for the first time from the viewpoint of asymmetry, although gluing bifurcation as a homoclinic bifurcation of codimension-2 has recently been studied [20] in

the perspective of asymmetry. It is already known that the homoclinic bifurcation is an important mechanism of spiking and bursting in neuron models. From this viewpoint, the observed bursting regimes will be investigated with much rigor in future.

References

[1] S Wiggins, *Introduction to applied nonlinear dynamical systems and chaos* (Springer-Verlag, NY, 1990)
[2] Y A Kuznetsov, *Elements of applied bifurcation theory* (Springer-Verlag, NY, 1995)
[3] V Petrov, S K Scott and K Showalter, *J. Chem. Phys.* **97**, 6191 (1992)
[4] T Peacock and T Mullin, *J. Fluid. Mech.* **432**, 369 (2001)
[5] A N Pisarchik, R Meucci and F T Arecchi, *Eur. Phys. J.* **D13**, 385 (2001)
[6] E Allaria, F T Arecchi, A Di Garbo and M Meucci, *Phys. Rev. Lett.* **86**, 791 (2001)
[7] R Herrero, R Pons, J Farjas, F Pi and G Orriols, *Phys. Rev.* **E53**, 5627 (1996)
[8] J J Healy, D S Broomhead, K A Cliffe, R Jones and T Mullin, *Physica* **D48**, 322 (1991)
[9] R R Llinás, *Science* **243**, 1654 (1988)
[10] M Breakspear, J R Terry and K J Friston, *Network: Computation in Neural Computing* **14**, 703 (2003)
[11] V N Belykh, I V Belykh, M Colding-Jorgensen and E Mosekilde, *Eur. Phys. J.* **E3**, 205 (2000)
[12] A L Shilnikov and N F Rulkov, *Int. J. Bifurcat. Chaos* **13**, 3325 (2003)
[13] E M Izhikevich, *Int. J. Bifurcat. Chaos* **10**, 1171 (2000)
[14] I P Marino, E Allaria, R Meucci, S Boccaletti and F T Arecchi, *Chaos* **13**, 286 (2003)
[15] P Glendinning and C Sparrow, *J. Stat. Phys.* **l35**, 645 (1984)
[16] P Gaspard and X-J Wang, *J. Stat. Phys.* **48**, 151 (1987)
[17] Marc T M Koper, *Physica* **D80**, 72 (1995)
[18] A Goryachev, P Strizhak and R Kapral, *J. Chem. Phys.* **107**, 2881 (1997)
[19] S Rajesh and G Ananthakrishna, *Physica* **D140**, 193 (2000)
[20] P Glendinning, J Abshagen and T Mullin, *Phys. Rev.* **E64**, 036208 (2001)
[21] L O Chua, M Komuro and T Matsumoto, *IEEE Trans. Cir. Systs.* **CAS-33**, 1072 (1986)
[22] M P Kennedy, *IEEE Trans. Cir. Systs.* **CAS-40**, 657 (1993)
[23] S K Dana and S Chakraborty, *Int. J. Bifurcat. Chaos* **14**, 1375 (2004)